Ionics (2024) 30:3745–3753
https://doi.org/10.1007/s11581-024-05530-4

RESEARCH

Double-layered SnO_2@NC hollow spheres as anode materials for high-performance lithium-ion batteries

Jin'an Zhao[1,3] · Liyun Dang[2] · Jiyong Hu[2] · Yan Guo[2]

Received: 6 February 2024 / Revised: 29 March 2024 / Accepted: 10 April 2024 / Published online: 26 April 2024

Abstract

Tin dioxide-based high-performance anode materials for lithium-ion batteries have been a hot research topic in recent years. In this study, nitrogen-doped and double-layered SnO_2@NC hollow spheres were prepared via simple and convenient method using carbon spheres as template. A series of products were obtained by varying additive amount of dopamine. When tested in the current density of 400 mA g^{-1}, SnO_2@NC-3 can provide a robust reversible capacity of 697.7 mAh g^{-1} after 270 cycles. The discharge capacity can remain 640.8 mAh g^{-1} after 800 cycles at 1000 mA g^{-1}. Above excellent electrochemical properties were attributed to the synergistic effect between nitrogen-doped carbon and nanosized-SnO_2 particles. The hollow structure can not only effectively buffer the structure crushing of the electrode in the process of charge and discharge, but also facilitate the electron diffusion by improving the electronic conductivity. Therefore, the unique nitrogen-doped and double-layered tin dioxide is a promising anode material for lithium-ion battery.

Keywords Lithium ion battery · Hollow spheres · Carbon coating · Anode material

Introduction

Lithium-ion batteries (LIBs) are critical portable electronic power sources with high energy density, long cycle life and low self-discharge [1–3]. In order to meet the increasing demand for large-scale applications, especially in the field of transportation, there are still high expectations for new electrode materials with high energy density and long-term cycling stability [4, 5]. However, with the rapid development and growth of energy demand, the commercial graphite with a theoretical specific capacity of 372 mAh g^{-1} has been unable to meet the increasing demand for battery capacity [6, 7]. Thus, it is the pursuit of scientific researchers to explore novel anode materials with higher theoretical specific capacity to meet the urgent requirements.

As one of the most competitive candidates for lithium-ion batteries, SnO_2 has attracted much attention on account of its abundant resources, high theoretical specific capacity, and low working potential [8–10]. Furthermore, the voltage window of SnO_2 electrode matches well with the positive electrode material, which guaranteed wider application range [11, 12]. However, in the electrode reaction, poor electronic conductivity and serious volume change (~359%) will inevitably lead to electrode disintegration and other problems, further reducing its capacity, cycle performance, and rate performance [13]. In addition, the pulverization and shedding of active substances will occur in the process of discharge–charge cycle, which will destroy the solid electrolyte interface (SEI), resulting in rapid capacity attenuation, and severely limiting its application in life. [14]

Various strategies have been devoted to overcome above problems for decades and kinds of tactics have been proposed. One effective approach is to design materials with nano/microstructure hierarchies to take the advantages of relatively stable microstructure, short diffusion path, and

Jin'an Zhao and Liyun Dang contributed equally to this work.

✉ Jin'an Zhao
zjinan@zzu.edu.cn

✉ Liyun Dang
20161010@huuc.edu.cn

[1] School of Pharmacy and Chemical Engineering, Zhengzhou University of Industrial Technology, Zhengzhou 451100, Henan, China

[2] College of Material and Chemical Engineering, Henan University of Urban Construction, Pingdingshan 467036, Henan, China

[3] College of Chemistry, Zhengzhou University, Zhengzhou 450001, Henan, China

large interfacial contact area, which is benefit for excellent rate capacity, better cycling performance, and improved lithium storage capacity. [15, 16] Tong group fabricated tube-in-tube SnO_2 superstructure with high specific surface area and sufficient volume, which supplied enough room for buffering volume changing during Li insertion and extraction and exhibited excellent discharge capacity when evaluated as lithium-ion battery anode. [17]

Another approach is to enhance electronic conductivity of SnO_2 electrode. In recent years, various carbon-based substrates have been widely reported for encapsulation or recombination of SnO_2 active materials, including graphene, carbon black, carbon nanotubes, carbon nanofibers, and carbon frames [18–20]. Furthermore, the agglomeration of nanomaterials electrode is alleviated with the introduction of carbon component. Notohara group synthesized SnO_2/SWCNT nanocomposite in a vacuumed glass using SWCNT and $SnCl_2$ as raw material. The nanoconfinement structure of SnO_2 nanoparticles in SWCNT limited the volume change and is benefit for reversible electrode reaction [21]. The introduction of nitrogen atoms into the carbon layer will produce more defects, providing more active sites for lithium storage, thus nitrogen-doped carbon (NC) can effectively improve electron conductivity in carbon materials [22]. Liang group reported a simple route to obtain nitrogen-doped graphene/SnO_2 composite. Nitrogen doping in graphene give rise to good conductivity, simultaneously compensates defects of pure SnO_2, and displayed higher lithium storage capacity and good cycling stability [23].

In this paper, nitrogen-doped and double-layered porous SnO_2 hollow spheres are prepared by electrostatic adsorption between negatively charged carbonaceous microspheres (CMS) template and positive metal cation (Sn^{4+}) followed by annealing treatment. The porous SnO_2 hollow spheres are loaded with nitrogen-doped carbon (NC) by deposition reaction. The double-layered SnO_2@NC-3 electrode materials delivered high specific capacity of 697.7 mAh g^{-1} at 400 mA g^{-1} after 270 cycles. What's more, the SnO_2@NC-3 composite materials reveal outstanding cycling stability under high current density (640.8 mAh g^{-1} at 1000 mA g^{-1} after 800 cycles).

Experimental section

Synthesis and treatment of carbon spheres

Synthesis of carbon spheres: 2 g glucose was dissolved in 32 mL water. Subsequently, the solution was transferred to a 40-mL autoclave at 170 °C for 12 h in an oven. After the reaction, the product was naturally cooled to room temperature, washed several times with water and ethanol, and dried at 80 °C in the oven. Alkali-treated carbonaceous microspheres: a certain quantity of carbon spheres was added to 0.05 M sodium hydroxide solution followed by stirring for a certain time at room temperature and drying at 80 °C for 12 h.

Synthesis of hollow SnO_2

The 0.6 g alkali-treated carbonaceous microspheres were dispersed in 1 M $SnCl_4{\cdot}5H_2O$ solution for ultrasonic dispersion, and the resulting suspension was aged at room temperature for 4 h, filtered, washed and dried at 80 °C for 12 h. Then the obtained alkaline carbon spheres were calcined at 700 °C in the air to obtain white products, which was named SnO_2.

Synthesis of double layered SnO_2@NC

In a typical process, 0.08 g hollow SnO_2 and 0.24 g dopamine were stirred in 25 ml of Tris buffer for 24 h. The SnO_2@polydopamnine hollow balls were centrifuged and carbonized in an N_2 atmosphere at 600 °C for 2 h (denoted as SnO_2@NC-3). The SnO_2@NC-2 and SnO_2@NC-1 samples were synthesized via the identical process by adapting the content of dopamine.

Material characterization

The crystal structures of the as-prepared samples were studied using X-ray diffraction (XRD) on Shimadzu XRD-6100 powder with Cu Kα radiation (λ = 1.5406 Å). The morphology of the samples and elemental distribution was obtained by transmission electron microscope (TEM, JEOL JEM-2100). Scanning electron microscopy (SEM) images were obtained on Hitachi S-4800 field emission microscope equipped with an X-ray energy dispersive spectrometer (EDS), and X-ray photoelectrons (XPS) was conducted on ESCALAB 250 system to analyze element composition and surface element states.

Electrochemical measurements

First of all, active material, cochin black, and polyvinylidene fluoride (PVDF) were mixed with a mass ratio of 70: 20: 10 in N-methyl-2-pyrrolidone (NMP). The resultant slurry was coated on copper foil and dried in a vacuum cabinet at 100 °C for 12 h. The mass loading calculated was approximately 0.6–0.8 mg cm^{-2}. Lithium sheet was used as the counter electrode and polyethylene (PE) film as the separator. 1 M $LiPF_6$ dissolved in ethylene carbonate, dimethyl carbonate, and ethylmethyl carbonate (1:1:1, in volume ration) was employed as the electrolyte. The half cells were assembled in a glove box filled with highly pure argon (H_2O, O_2 < 0.3 ppm, Etelux) using CR 2032-coin cells. The

charge–discharge measurement was tested on LAND CT-2001A (Wuhan, China). Cyclic voltammetry (CV) measurements were employed in the voltage range of 0.01–3.0 V with a scan rate of 0.1 mV s^{-1} in RST5000 electrochemical workstation. Electrochemical impedance spectroscopy (EIS) measurements of cells were also recorded on RST 5000 electrochemical workstation over a frequency range of 100 kHz to 0.01 Hz.

Results and discussion

Material synthesis and characterization

The synthesis diagram of double-layer SnO_2@NC was shown in Fig. 1. Variation of dopamine from 0.08 g, 0.16 g, to 0.24 g give rise to three products, SnO_2@NC-1, SnO_2@NC-2, and SnO_2@NC-3, respectively.

The XRD spectrums of the synthesized SnO_2@NC composite and SnO_2 were shown in Fig. 2a. The sharp diffraction peaks at 2θ values of 26.61°, 33.89°, 37.94°, 51.78°, 54.75°, and 62.59° were corresponded to (110), (101), (200), (211), (220), and (221) planes of tetragonal rutile SnO_2, which matches well with JCPDS card No.41–4451 [24, 25]. After careful observation, there was still a small amount of carbon remaining in the SnO_2 sphere, the typical bulging peak of carbon appears at about 20°. From the XRD results of SnO_2@NC-3, SnO_2@NC-2, and SnO_2@NC-1, the intensity of the SnO_2 peak became stronger than SnO_2 sphere, which can be ascribed to better crystallinity at higher temperature after calcination under N_2 atmosphere. No obvious coexisting carbon peaks were observed, which was supposed to amorphous carbon produced by the carbonization of polydopamine. The surface electronic state and composition of the as-prepared SnO_2@NC-3 was detected by XPS in Fig. 2b–2f. The full XPS spectrum of SnO_2@NC-3 in Fig. 2b included Sn, N, C, and O elements. Peaks at 495.3 eV and 486.9 eV in the fine spectrum of Sn $3d_{3/2}$ and Sn $3d_{5/2}$ manifested the formation of SnO_2 in Fig. 2c. [26] A symbolic spin energy separation of 8.4 eV in Fig. 2c corresponds well to the Sn (IV)

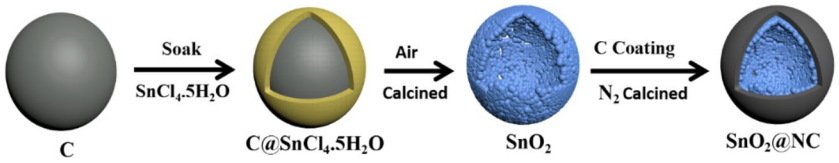

Fig. 1 Composite schematic diagram of double layered SnO_2@NC

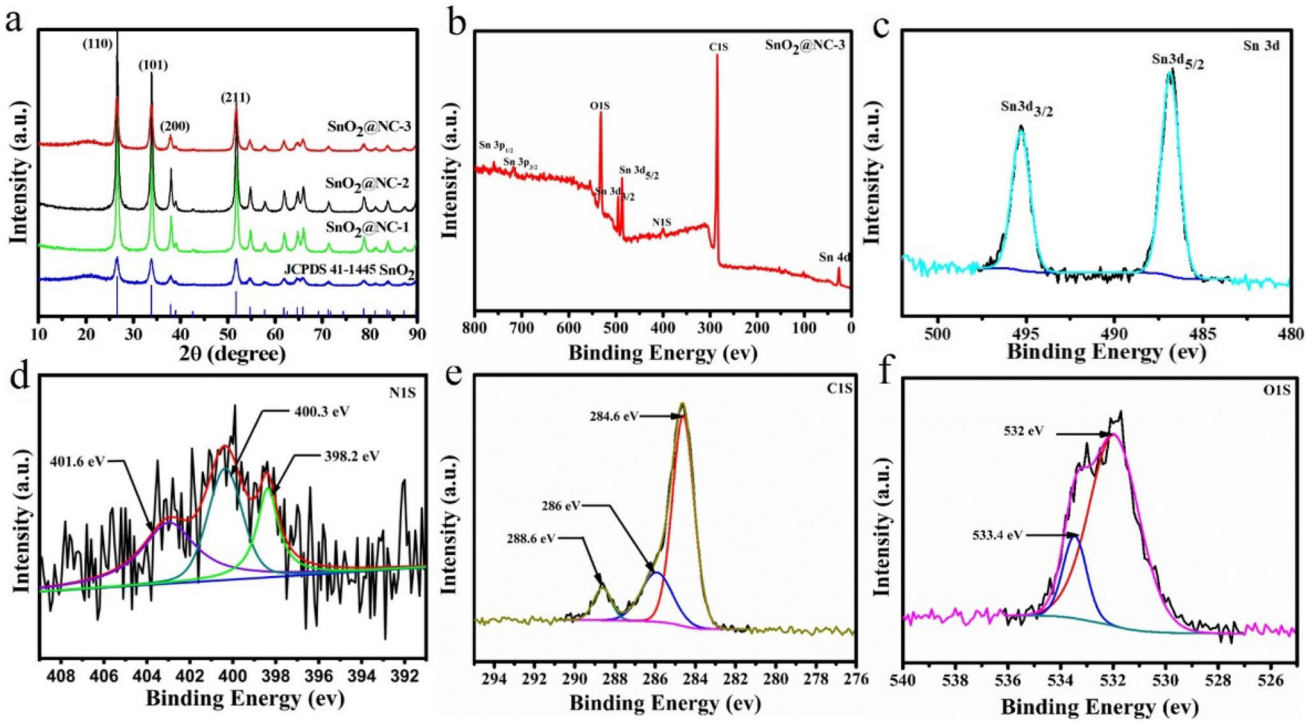

Fig. 2 **a** XRD patterns of SnO_2@NC-3, SnO_2@NC-2, SnO_2@NC-1, and SnO_2; **b** full XPS spectra of SnO_2@NC-3; high-resolution spectra of **c** Sn 3d, **d** N 1 s, **e** C 1S, and **f** O 1S

oxidation state of SnO_2 [27–29] .High resolution peak of N in Fig. 2d demonstrated the three forms of nitrogen element, which are pyridinic N (398.2 eV), pyrrolic N (400.3 eV), and graphitic N (401.6 eV), respectively [30, 31]. N-doped carbon can provide sufficient defects and active sites, which inevitably improve lithium storage capacities [32]. As shown in Fig. 2e, the C1s spectrum can be divided into three peaks corresponding to the 284.6, 286, and 288.6 eV of C–C (sp^2 C), C = O, and O-C = O groups, respectively [33, 34] .The peak of C1s was mainly due to the nitrogen-doped carbon outside SnO_2 nanoparticle. In the Fig. 2f, the O1s binding energy of SnO_2 was 532 eV, corresponding to the typical Sn–O bond binding energy. Meanwhile, the peak at 533.4 eV was ascribed to C–O–C bond. Full XPS spectrum and fine spectrums of SnO_2 were shown in Fig. S1, which demonstrated the existing of Sn–O bonds.

The morphology and detail structure of the prepared SnO_2 samples were characterized by SEM and TEM. It can be seen from Fig. 3a–b that the carbon spheres synthesized by hydrothermal method were of uniform size and good dispersion, with a diameter of 600–700 nm. From the SEM images of SnO_2 formed by calcination of tin salt-soaked carbon sphere in Fig. 3c–d, uniformly SnO_2 hollow spheres were detected clearly. Subsequent TEM images of SnO_2 were presented in Fig. 3e–f, from which hollow sphere structures were confirmed and porous sphere shell accumulated by many small particles can also be observed distinctly. The crystal structure of SnO_2 was measured by HRTEM in Fig. 3g. A clear lattice fringe of approximately 0.33 nm was detected in the image, which matches well with the (110) plane of SnO_2. [35, 36] The selected area electron diffraction (SAED) patterns of SnO_2 showed characteristic diffraction rings in Fig. 3h, which demonstrated the rutile structure of SnO_2 and polycrystalline state of the material. Above results were in good accordance with XRD results, indicating the polycrystalline structure of the product.

Using dopamine as carbon source to carbonize polycrystalline SnO_2, variation of dopamine additive amount leading to three products, as is shown in Fig. 4. From Fig. 4a, a layer of nitrogen doped carbon (NC) can be detected on the surface of hollow SnO_2, which maintained the hollow morphology. As shown in Fig. 4b, when the amount of dopamine was 0.16 g, the NC coating layer loaded on SnO_2 surface was thicker than that of 0.08 g dopamine. When the amount of dopamine was increased to 0.24 g, the hollow tin dioxide has been completely wrapped by nitrogen-doped carbon, forming an intact spherical structure in the Fig. 4c. From the above analysis, it can be speculated that with the continuous increase of dopamine content, the nitrogen doped carbon on the surface of hollow SnO_2 spheres became more and more, until the hollow tin dioxide spheres were completely enveloped, forming a spherical double-layered tin dioxide hollow sphere structure. Corresponding TEM pictures in Fig. 4d–4f displayed the same tendency of thicker carbon layer with more dopamine additive amount. Selected area electron diffraction pattern of brown circle in TEM picture

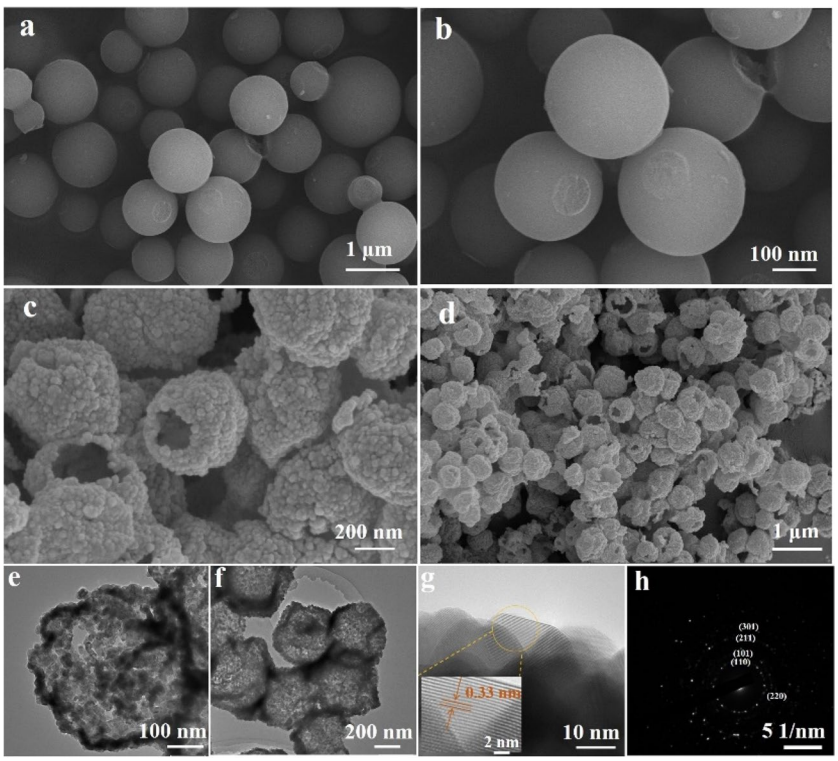

Fig. 3 **a**, **b** SEM images of carbon spheres; **c**, **d** SEM image, **e**-**h** TEM and SAED pattern of as-prepared SnO_2 hollow nanospheres

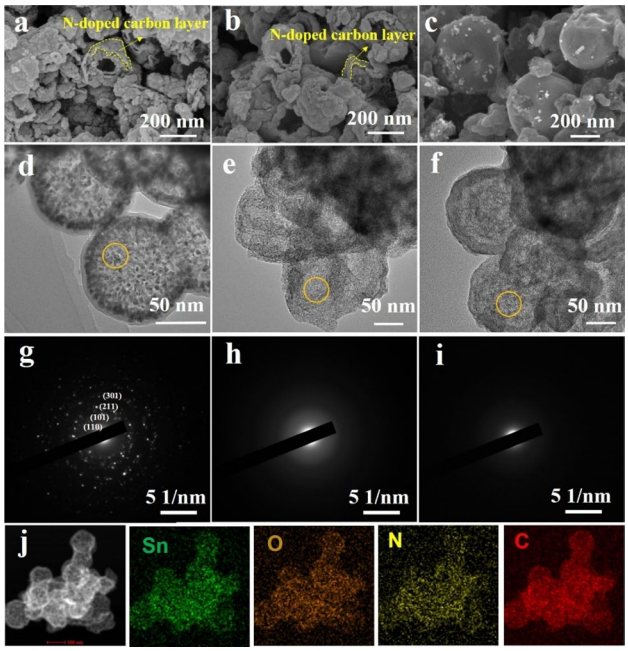

Fig. 4 SEM, TEM pictures, and SAED patterns of **a**, **d**, **g** SnO_2@NC-1; **b**, **e**, **h** SnO_2@NC-2; **c**, **f**, **i** SnO_2@NC-3; and **j** elemental mappings of SnO_2@NC-3

was presented in Fig. 4g–i. From Fig. 4g, typical polycrystal diffraction points were observed and amorphous diffraction ring appeared with the thickening of carbon layer as shown in Fig. 4h and i. The EDX spectrum SnO_2@NC-3 in Fig.S2 revealed the presence of C, O, Sn, and N peaks in SnO_2@NC-3, implying that nitrogen-doped carbon has been successfully loaded on the surface of SnO_2. Figure 4j presents the elemental mapping images of SnO_2@NC-3 electrode, from which uniform distribution of Sn, O, C, and N can be clearly observed, representing even carbon coating on the surface of SnO_2 and good integrity of electrode materials.

The electrochemical characterization of the SnO_2@NC-3 composite was investigated in Fig. 5. From Fig. 5a, the CV curves of the composite were obtained in a range from 0.1 to 3.0 V at a scanning rate of 0.1 mV s^{-1}. During the initial anode scan, a sharp and wide peak at 0.5 V was observed, which was ascribed to dealloying, while the two peaks at 1.25 and 1.91 V corresponded to the oxidation of SnO_2 [37, 38]. In the initial cathodic scanning, the reduction reaction at the peaks of 0.9 V represented the lithiation reaction of SnO_2: $\mathbf{SnO_2 + 4Li^+ + 4e^- \rightarrow Sn + 2Li_2O}$. The peak at about 0.2 V was attributed to the lithiation reaction of Sn:$\mathbf{Sn + xLi^+ + xe^+ \rightarrow Li_xSn}(0 \leq x \leq 4.4)$ [39, 40]. In addition, the unique peak at about 0.71 V revealed the lithiation of SnO_2 and the irreversible formation of the SEI (solid electrolyte intermediate phase) layer [41]. However, the peak density gradually decreases during the cycle, indicating the irreversible nature. The SEI film formed during the first cycle is beneficial to the stability of the anode material structure and improvement of electrochemical performance. The following CV curves were almost overlapping, thus verifying the good reversibility of the SnO_2@NC-3 composite.

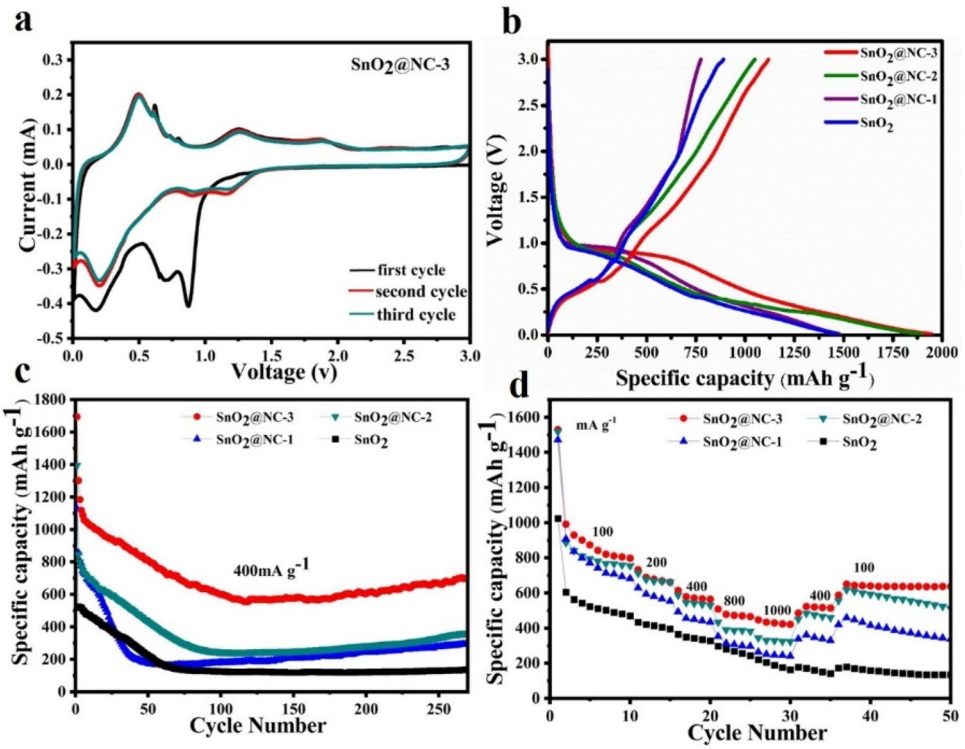

Fig. 5 **a** Cyclic voltammetry curve of SnO_2@NC-3; **b** Charge/discharge curves at a current density of 100 mA g^{-1}; **c** Cycling performance at a current density of 400 mA g^{-1}; **d** Rate capabilities at different current densities of SnO_2, SnO_2@NC-1, SnO_2@NC-2, and SnO_2@NC-3 electrodes

Figure 5b disclosed the first charge and discharge curves of SnO_2@NC-1, SnO_2@NC-2, SnO_2@NC-3, and SnO_2 electrodes at a current density of 100 mA g^{-1}. The first cycle discharge specific capacities of SnO_2@NC-3, SnO_2@NC-2, SnO_2@NC-1, and SnO_2 electrode materials were 1944.3, 1894.8, 1479.5, and 1470.8 mAh g^{-1}, respectively.

When tested at a current density of 400 mA g^{-1}, SnO_2@NC-3 can provide a high reversible capacity of 697.7 mAh g^{-1} after 270 cycles, which was distinctly higher than SnO_2@NC-1 (294 mAh g^{-1}), SnO_2@NC-2 (362.9 mAh g^{-1}), and SnO_2 (137.7 mAh g^{-1}) in Fig. 5c, showing excellent cycling stability. In order to further study the differences in the electrochemical performance of SnO_2@NC-1, SnO_2@NC-2, SnO_2@NC-3, and SnO_2, rate performance tests were carried out on four samples. The rate capabilities of the as-obtained samples were displayed in Fig. 5d, the SnO_2@NC-3 electrode delivered discharge capacities of about 990.9, 689.2, 579.3, 478.4, and 433.8 mAh g^{-1} at increasing current rates of 100, 200, 400, 800, and 1000 mA g^{-1}, respectively. Furthermore, a high capacity of the electrode can be backed to 650.4 mAh g^{-1} when the current was rebounded to 100 mA g^{-1}, while SnO_2@NC-2, SnO_2@NC-1, and SnO_2 showed the discharge specific capacity of 906, 593.6, 455.4, 313.8, 250.2 mAh g^{-1}; 886.3, 676.9, 546.1, 390.6, 331.8 mAh g^{-1}; and 604.8, 421.3, 349.4, 208.6, 204.2 mAh g^{-1} respectively. Rate performance test of SnO_2@NC-3 electrode showed step-sensitive changes under different current densities; furthermore, higher discharge capacities implied better stability than SnO_2@NC-2, SnO_2@NC-1, and SnO_2 electrode materials.

Long-cycle stability of all samples was tested at a high current density of 1000 mA g^{-1} in Fig. S3a; the double layered SnO_2@NC-3 can provide a high capacity of 640.8 mAh g^{-1} after 800 cycles. The reversible capacity was significantly superior to SnO_2@NC-2 (235.1 mAh g^{-1}), SnO_2@NC-1 (192.5 mAh g^{-1}), and SnO_2 (146.9 mAh g^{-1}). It can be seen from Fig. S3a that the discharge specific capacity of the four electrode materials showed a downward trend before 100 cycles; however, after 100 cycles, the discharge specific capacity exhibited an upward trend. The full immersion of active material in electrolyte and activation of electrode in previous loop give rise to upward tendency, which is benefit for the maintenance of capacity [42]. The reversible capacity degradation of SnO_2@NC-1, SnO_2@NC-2, and SnO_2 electrodes has a more severely decline than that of SnO_2@NC-3, on account of the instability of the electrode structure and the formation of thicker SEI film. Finally, the long-cycle stability of SnO_2@NC-3 under an ultra-high current density of 5000 mA g^{-1} was shown in Fig. S3b; the double layered SnO_2@NC-3 still can maintain a discharge capacity of 212.7 mAh g^{-1} after 1000 cycles, with 100% Coulombic efficiency. According to the description of above results, SnO_2@NC-3 exhibited excellent cycling stability, which was more suitable for large current charging and discharging.

There were two main reasons for the high reversible capacity of the SnO_2@NC-3 electrode material: One reason was the advantage of the hollow sphere structure of interior SnO_2, which was accumulated by small nanoparticles of SnO_2. Nanosized SnO_2 crystal can fully contact with the electrolyte to improve the reversibility of the reaction, and the hollow sphere structure can relieve the volume expansion in the process of charge and discharge. Another reason was the introduction of nitrogen doped carbon. Nitrogen doped carbon coated on the surface of SnO_2 hollow spheres can not only inhibit the volume effect of SnO_2 nanocrystals during cycling, but also prevent the accumulation of SnO_2. Meanwhile, it can also improve the formation and decomposition of SEI films to prevent the capacity decline caused by the formation of thicker SEI films.

More importantly, nitrogen-doped carbon can significantly improve the conductivity of the electrode material, and ultimately improved the electrochemical performance of the SnO_2@NC-3. It can be speculated from the above analysis that the amount of carbon content has a great influence on the electrochemical performance of battery materials. More amount of nitrogen-doped carbon coating on the surface of the hollow SnO_2 is conducive to alleviate the large volume expansion and the crushing and shedding charge/discharge process of active materials. Thus, SnO_2@NC-3 electrode material (dopamine addition was 0.24 g) has excellent electrochemical performances.

To further investigate the transmission kinetics of electrons and ions promoted by the designed multilayer hollow structure, electrochemical impedance spectroscopy was performed on half-cells under the test frequency ranges from 100 kHz to 0.01 Hz in Fig. 6a, which showed that each plot was composed of semicircles (high frequency region) and straight lines (low frequency region). After calculation, the Rct of SnO_2@NC-3 electrode was about 84.86 Ω, which was lower than SnO_2@NC-1 (103 Ω), SnO_2@NC-2 (86.07 Ω), and SnO_2 (193 Ω). The relatively low charge transfer resistance of SnO_2@NC-3 can accelerate the ion migration between the electrolyte and the active material, which accelerated electrode reaction and generated better electrochemical performance.

In the low frequency region, the slope value σ in Fig. 6b can be obtained by Eq. (1): [43, 44].

$$Z\prime = R_D + R_L + \sigma\omega^{-1/2} \tag{1}$$

After calculation, the slope of the SnO_2@NC-3 was 25.44, which was smaller than SnO_2@NC-2 (30.54), SnO_2@NC-1 (186.43), and SnO_2 (350.54), indicating SnO_2@NC-3 was more conducive to the diffusion of Li^+ between active material particles and electrolyte. This result was consistent

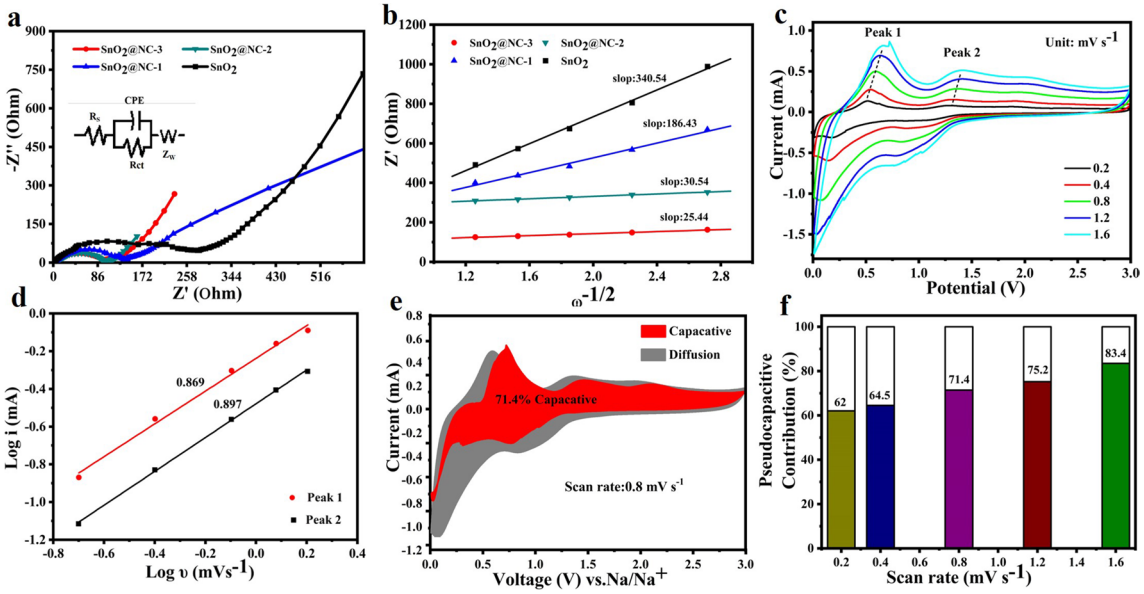

Fig. 6 **a** Nyquist diagram in the frequency range of 0.01 Hz–100 kHz and **b** Z'-$\omega^{-1/2}$ curve in the low-frequency range of SnO_2@NC-3, SnO_2@NC-2, SnO_2@NC-1, and SnO_2; diagrams of SnO_2@NC-3: **c** CV curves at different scanning rates; **d** The line relationship of log(i) vs. log(v); **e** capacitive contribution at the scan rate of 0.8 mV s^{-1}; **f** Comparison of the pseudocapacitive contribution under different sweeping rates

with the excellent electrochemical performance of SnO_2@NC-3.

The cyclic voltammetry curves at different scan rates of SnO_2@NC-3 (in a voltage window of 0.01 to 3 V) were shown in Fig. 6c; the pseudocapacitance behavior was discussed and capacitance contribution can be evaluated by Eq. (2): [45, 46].

$$\log(i) = \mathrm{b}\log(v) + \log(a) \tag{2}$$

The value of a is an empirical parameters and b can be calculated from the slope of the linear relationship between log*i* and log*v* in Fig. 6d. The b value close to 0.5 discloses a diffusion-controlled behavior and the b value close to 1 demonstrates an excellent pseudocapacitive behavior. As shown in Fig. 6d, the b-value for peak 1 and peak 2 was 0.869 and 0.897, respectively, manifesting that the diffusion-controlled and pseudocapacitive behaviors were responsible for the high capacity of SnO_2@NC-3. Therefore, we can reasonably infer that the two processes contributed to the total capacity.

The contribution of capacitance to total lithium storage capacity can be quantitatively calculated by Eq. (3): [47–49].

$$i(v) = k_1\mathrm{v} + k_2 v^{1/2} \tag{3}$$

In Eq. (3), $i(v)$ is the total current value, meanwhile the values of $k_1 v$ and $k_2 v^{1/2}$ reflect the pseudocapacitive and diffusion-controlled process, respectively. From Fig. 6e, the capacitive contribution of SnO_2@NC-3 electrode was ~ 71.4% at a scan rate of 0.8 mV s^{-1}. When the scan rates ascended from 0.2 to 1.6 mV s^{-1} in Fig. 6f, the percentage of the pseudocapacitive contribution increased from 62 to 83.4%. It can be concluded that capacitive behavior was beneficial to predominant capacity for the enhanced cycling stability and rate performances.

Conclusions

SnO_2@NC composite material was synthesized by simple hydrothermal and deposition reactions. Polydopamine was successfully loaded on the surface of SnO_2 through a deposition reaction and carbonized under the protection of N_2 atmosphere. Carbon stabilized the electrode structure and improved the charge transfer ability of active material, which are responsible for better electrochemical performance. The introduction of nitrogen atoms in carbon skeleton can bring in more defects and active sites. N-doped carbon coating on the surface of SnO_2 prominently alleviate volume effect, which is beneficial to the propagation and diffusion of Li^+. Moreover, hollow interior provided sufficient room for volume change because of insertion and extraction of Li^+ during electrode reaction. In conclusion, SnO_2@NC-3 electrode can retain a reversible capacity of 640.8 mAh g^{-1} after 800 cycles at a current density of 1000 mA g^{-1} and displayed steady cycling stability. Furthermore, rate evaluation of SnO_2@NC-3 electrode at different current densities also demonstrated best and most flexible response. The above

results well proved that the double layered SnO_2@NC-3 hollow sphere was a potential and prospective anode material for lithium-ion batteries.

Supplementary Information The online version contains supplementary material available at https://doi.org/10.1007/s11581-024-05530-4.

Author contribution Jin'an Zhao: Methodology, Software, Investigation, Writing-original draft. Liyun Dang: Conceptualization, Supervision. Jiyong Hu: Resources, Validation, Formal analysis. Yan Guo: Software, Methodology.

Funding This study was funded by College students' innovation and entrepreneurship training (202311765015), Henan Key Science and Technology Research (242102230104), and Postgraduate Education Reform and Quality Improvement Project of Henan Province (YJS2023JD65).

Data availability The data presented in this paper are available on request from the corresponding author.

Declarations

Ethics approval This work did not include any studies involving humans or animals.

Competing interests The authors declare no competing interests.

References

1. Liu X, Zhang S, Zhang P, Zheng ZM, Bai F, Li Q (2023) Integrated structure design and synthesis of a pitaya-like SnO_2/N doped carbon composite for high-rate lithium storage capability. Nanoscale 15:1669–1675
2. Tu Z-Y, Choudhury S, Zachman M-J, Wei S-Y, Zhang K-H, Kourkoutis L-F, Archer L-A (2018) Fast ion transport at solid-solid interfaces in hybrid battery anodes. Nat Energy 3:310–316
3. Kim H, Kim H, Ding Z, Lee M-H, Lim K, Yoon G, Kang K (2016) Recent progress in electrode materials for sodium-ion batteries. Adv Energy Mater 16:943–981
4. Benedek P, Forslund O, Nocerino E, Yazdani N, Matsubara N (2020) Quantifying diffusion through interfaces of lithium ion batteries active materials. ACS Appl Mater Interfaces 12:16243–16249
5. Yin S-J, Zhang X-Q, Liu D-D, Huang X-X, Wang Y-S, Wen G-W (2024) Synthesis of heterointerfaces in NiO/SnO_2 coated nitrogen-doped graphene for efficient lithium storage. Phys Chem Chem Phys 26:3415–3423
6. Liu Y-W, Sun S-W, Han J, Gao C, Fan L, Guo R (2021) Multi-yolk–shell MnO@Carbon nanopomegranates with internal buffer space as a lithium ion battery anode. Langmuir 37:2195–2204
7. Tian W-H, Bai P, Wang Z-H, Ling G-Q, Ren J, Ren R-P, Lv Y-K (2023) CdS@C nanowires with rich sulfur vacancies for high-performance lithium storage anodes. Ionics. https://doi.org/10.1007/s11581-023-05345-9
8. Cui Z-P, Sun M, Liu H-Q, Li S-J, Zhang Q-Y (2020) Double-shell SnO_2@Fe_2O_3 hollow spheres as a high-performance anode material for lithium-ion batteries. CrystEngComm 22:1197–1208
9. Zhang X-Q, Huang X-X, Zhang X-D, Xia L, Zhong B, Zhang T, Wen G-W (2016) Flexible carbonized cotton covered by graphene/Co-doped SnO_2 as free-standing and binder-free anode material for lithium-ions batteries. Electrochim Acta 222:518–527
10. Hu R-Z, Ouyang Y-P, Chen D-C, Wang H, Chen Y, Zhu M, Liu M-L (2016) Inhibiting Sn coarsening to enhance the reversibility of conversion reaction in lithiated SnO_2 anodes by application of super-elastic NiTi films. Acta Mater 109:248–258
11. Zhan L, Zhou X, Luo J, Ning X (2019) Binder-free multilayered SnO_2/graphene on Ni foam as a high-performance lithium ion batteries anode. Ceram Int 45:6931–6936
12. Wu C-H, Zhu G-J, Wang-Q W-H, Zhang H-J (2021) A novel route to prepare N-graphene/SnO_2 composite as a high-performance anode for lithium batteries. Energy Storage Mater 43:430–462
13. Etacheri V, Seisenbaeva G-A, Caruthers J, Daniel G, Nedelec J-M, Kessler V-G, Pol V-G (2015) Ordered network of interconnected SnO_2 nanoparticles for excellent lithium-ion storage. Adv Energy Mater 5:1401289
14. Dai Y, Li F, Fu Y-X, Mo D-C, Lyu S-S (2021) Carbon-coated SnO_2 riveted on a reduced graphene oxide composite (C@SnO_2/RGO) as an anode material for lithium-ion batteries. RSC Adv 11:8521–8529
15. Wang M-K, Chen T-R, Liao T-H, Zhang X-L, Zhu B, Tang H, Dai C-S (2021) Tin dioxide-based nanomaterials as anodes for lithium-ion batteries. RSC Adv 11:1200–1221
16. Zhao K, Zhang L, Xia R, Dong Y, Xu W, Niu C, He L, Yan M, Qu L, Mai L (2016) SnO_2 quantum dots@ graphene oxide as a high-rate and long-life anode material for lithium-ion batteries. Small 12:588–594
17. Tong Y-L, Dang L-Y, Wang Z-R, Zhang H, Gao F, Lu Q-Y (2019) Tube-in-tube tin dioxide superstructures with enhanced lithium storage performance. Chem Commun 55:2222
18. Xie F-R, Zhao S-Q, Bo X-X, Li G-H, Fei J-M (2023) A robust solvothermal-driven solid-to-solid transition route from micron SnC_2O_4 to tartaric acid-capped nano-SnO_2 anchored on graphene for superior lithium and sodium storage. J Mater Chem A 11:53–67
19. Abe J, Takahashi K, Kawase K, Kobayashi Y, Shiratori S (2018) Self-standing carbon nanofiber and SnO_2 nanorod composite as a high-capacity and high-rate-capability anode for lithium-ion batteries. ACS Appl Nano Mater 1:2982–2989
20. Boya V, Parakandy MP, Khasim SB, Pavan SV, Mantripragada RK, Bulusu VS (2022) Oxygen vacancies enable excellent electrochemical kinetics of carbon coated mesoporous SnO_2 nanoparticles in lithium ion batteries. Mater Adv 3:1617–1628
21. Hiroo N, Koki U, Isamu M (2023) Direct evidence of reversible SnO_2−Li reactions in carbon nanospaces. ACS Appl Mater Interfaces 15:30600–30605
22. Du F-X, Liu S-L, Li Y, Wang J-K, Zhang P (2023) Facile synthesis of MoS_2/N-doped carbon as an anode for enhanced sodium-ion storage performance. Ionics 29:5183–5193
23. Liang K, Zhao Z-W, Zhou X, Xu A-W (2018) A novel route to prepare N-graphene/SnO_2 composite as a high-performance anode for lithium batteries. Dalton Trans 47:10206–10212
24. Kang Y-R, Li Z, Xu K, He X-J, Wei S-X, Cao Y-M (2019) Hollow SnO_2 nanospheres with single-shelled structure and the application for supercapacitors. J Alloy Compd 779:728–734
25. Han M-S, Mu Y-B, Yu J (2020) Nanoscopically and uniformly distributed SnO_2@TiO_2/C composite with highly mesoporous structure and bichemical bonds for enhanced lithium ion storage performances. Mater Adv 1:421–429
26. Korusenko P-M, Nesov S-N, Bolotov V-V et al (2019) Structure and electrochemical characterization of SnO_x/Sn@MWCNT composites formed by pulsed ion beam irradiation [J]. J Alloy Compd 793:723–731
27. Chen W-H, Song K-N, Mi L-W, Feng X-M, Zhang J-M, Cui S-Z, Liu C-T (2017) Synergistic effect induced ultrafine SnO_2/graphene nanocomposite as an advanced lithium/sodium-ion batteries anode. J Mater Chem A 5:10027–10038

28. Hu R-Z, Ouyang Y-P, Liang T, Wang H, Liu J, Chen J, Yang C-H, Yang L-C, Zhu M (2017) Stabilizing the nanostructure of SnO_2 anodes by transition metals-a route to achieve high initial Coulombic efficiency and stable capacities for lithium storage. Adv Mater 29:1605006
29. Xiao X-W, Wang Z-Q, Yao W-L, Rao X-F, Zhang Q (2023) Nano Sn-SnO_x embedded in multichannel hollow carbon nanofibers: microstructure, reversible lithium storage property and mechanism. Appl Surf Sci 635:157739
30. Eng A-Y, Wang Y, Nguyen D-T, Tee S-Y, Lim C-Y-J et al (2021) Tunable nitrogen-doping of sulfur host nanostructures for stable and shuttle-free room-temperature sodium−sulfur batteries [J]. Nano Lett 21:5401–5408
31. Wang J, Zhu Y-H, Zhang C, Kong F-J, Tao S, Qian B, Jiang X-F (2019) Bimetal phosphide $Ni_{1.4}Co_{0.6}P$ nanoparticle/carbon@nitrogendoped graphene network as high-performance anode materials for lithium-ion batteries. Appl Surf Sci 485:412–422
32. Xiao X-W, Yao W-L, Yan T-T, Zhang W-Y, Zhang Q (2023) Hybrid CuSn nanosphere-functionalized Cu/Sn co-doped hollow carbon nanofibers as anode materials for sodium-ion batteries. Nanoscale 156:15405–15414
33. Huang Z-Q, Gao H-Y, Ju J, Yu J-G, Zhao Y (2020) Sycamore-fruit-like SnO_2@C nanocomposites: rational fabrication, highly reversible capacity and superior rate capability anode material for Li storage. Electrochim Acta 331:135297
34. Korusenko P-M, Nesov S-N, Bolotov V-V, Povoroznyuk S-N, Sten'kin Y-A, Pushkarev A-I, Fedorovskaya E-O, Smirnov D-A (2019) Structure and electrochemical characterization of SnO_x/Sn@MWCNT composites formed by pulsed ion beam irradiation. J Alloy Compd 15:723–731
35. Lu H, Wan Y, Wang T, Jin R, Ding P, Wang R, Wang Y, Teng C, Li L, Wang X, Zhou D, Xue G (2019) A high performance SnO_2/C nanocomposite cathode for aluminum-ion batteries. Mater Chem A 7:7213–7220
36. Notohara H, Urita K, Moriguchi I (2023) Direct evidence of reversible SnO_2–Li reactions in carbon nanospaces [J]. ACS Appl Mater Interfaces 15:30600–30605
37. Ke J, Feng Y-F, Yang B-W, Wu K-D, Deng X-Q, He M (2020) A sheet-like SnO_2@SiO_2/graphite composite as anode material with excellent performance for lithium-ion batteries. Int J Electrochem Sci 15:10173–10183
38. Zhang L, Wu H-B, Liu B, Lou X-W (2014) Formation of porous SnO_2 microboxes via selective leaching for highly reversible lithium storage. Energy Environ Sci 7:1013–1017
39. Feng Y-F, Bai C, Wu K-D, Dong H-F, Ke J, Huang X-P, Xiong D-P, He M (2020) Fluorine-doped porous SnO_2@C nanosheets as a high performance anode material for lithium ion batteries. J Alloy Compd 843:156085
40. Ma Q, Chen M-N, Fang Z (2024) Tunable composition of Sn/SnO_2@C composites for lithium-ion batteries. Mater Lett 357:135716
41. Zheng Y, Zhou T-F, Zhang C-F, Mao J-F, Liu H-K, Guo Z-P (2016) Boosted charge transfer in SnS/SnO_2 heterostructures: toward high rate capability for sodium-ion batteries. Angew Chem Int Edit 10:3408–3413
42. Cheng J-P, Xiong D-P, Jiang W-Q, Ye W-B, Song P (2024) SnO_2-MoO_2 nanoparticles coated on graphene oxide as a high-capacity, high-speed, long-life lithium-ion battery anode. Chem Phys Lett 835:140994
43. Zhou Y, Zhang M, Wang Q, Yang J, Luo X, Li Y, Du R, Yan X, Sun X, Dong C, Zhang X, Jiang F (2020) Pseudocapacitance boosted N-doped carbon coated Fe_7S_8 nanoaggregates as promising anode materials for lithium and sodium storage. Nano Res 13:691–700
44. Lin X-T, Li P, Shao L-Y, Shui M, Wang D-J, Long N-B, Ren Y-L, Shu J (2015) Lithium barium titanate: a stable lithium storage material for lithium ion batteries. J Power Sources 278:546–554
45. Fang G-Z, Wu Z-X, Zhou J, Zhu C-Y, Cao X-X, Cao T-Q, Chen Y-M, Wang C, Pan A-Q, Liang S-Q (2018) Observation of pseudocapacitive effect and fast ion diffusion in bimetallic sulfides as an advanced sodium-ion battery anode. Adv Energy Mater 8:1703155
46. Zhang S-G, Zhao H-P, Ma W-Y, Mi J, Zhu J-F, Liu J-L (2022) Insight to Se-doping effects on Fe_7S_8/carbon nanotubes composite as anode for sodium-ion batteries. J of Power Sources 536:231458
47. Sun R-M, Liu S-J, Wei Q-L, Sheng J-Z, Zhu S-H, An Q-Y, Mai L-Q (2017) Mesoporous NiS_2 nanospheres anode with pseudocapacitance for high-rate and long-life sodium-ion battery. Small 13:1701744–1701748
48. Cook J-B, Kim H-S, Yan Y, Ko J-S, Robbennolt S, Dunn B, Tolbert S-H (2016) Mesoporous MoS_2 as a transition metal dichalcogenide exhibiting pseudocapacitive Li and Na-Ion charge storage. Adv Energy Mater 6:1501937
49. Ge P, Hou H, Li S, Yang L, Ji X (2018) Tailoring rod-like $FeSe_2$ coated with nitrogen-doped carbon for high-performance sodium storage. Adv Funct Mater 28:1801765–1801712